Classical impulsive model for dissociation of diatomic molecules in direct simulation Monte Carlo

Han Luo, Israel B. Sebastião, Alina A. Alexeenko, and Sergey O. Macheret*
School of Aeronautics and Astronautics Engineering, Purdue University, West Lafayette, Indiana 47906, USA

(Received 5 June 2018; published 26 November 2018)

An implementation of the Macheret-Fridman (MF) dissociation model for the direct simulation Monte Carlo (DSMC) method is developed in this work. The model maintains the fundamental physical assumptions of the MF model, i.e., that high-energy collisions resulting in dissociation can be described by classical mechanics and are close to the impulsive limit, but also eliminates additional approximations of the MF model by using Monte Carlo sampling. Recent quasiclassical trajectory (QCT) calculations of N_2, O_2, and NO dissociation reactions and experimental measurements are used to validate the model. In general, the reaction rate constants and average vibrational energy removed at thermal equilibrium and nonequilibrium conditions are in good agreement with the QCT and experimental values. The discrepancies in the absolute values of thermal equilibrium rate constants found in some cases are shown to be caused by the underprediction of collision rates with the variable hard sphere model rather than by the MF model itself. QCT-calibrated collision rates combined with the MF dissociation model for the $N_2 + O$ colliding pair are shown to yield a very good agreement between the computed thermal equilibrium dissociation rates and the QCT results. The model is also evaluated by simulating shock tube experiments with oxygen. The present study suggests the possibility of using the model as the standard dissociation reaction model for nonequilibrium flows.

DOI: 10.1103/PhysRevFluids.3.113401

I. INTRODUCTION

The dissociation reaction is a fundamental process in chemical physics. The process is also important in applications such as combustions and plasma chemistry, as well as in high-speed flows including shock layer formed during atmospheric reentry and the plumes of rocket engines [1–3]. In many cases, the dissociation occurs in thermal nonequilibrium conditions. For example, in hypersonic reentry, the large kinetic energy of the cold free stream is converted rapidly to the translational energy of molecules behind the shock front, whereas the vibrational mode of the molecules is excited at a rate lower by two to three orders of magnitudes. Thus, the dissociation starts in vibrationally cold conditions, the reaction rates are reduced, and the heat load on the vehicles surface is increased. In plasma chemistry, the opposite regime is realized: the dissociation reaction can occur at room temperature due to the presence of vibrationally hot molecules produced in collisions with electrons [4]. Due to the importance of the nonequilibrium dissociation reaction in practical applications, accurate modeling of this process is needed.

Computational fluid dynamics (CFD) and direct simulation Monte Carlo (DSMC) are the two principal methods to simulate such flows. The CFD method is based on numerical solution of Navier-Stokes equations. The internal energy of the gas is described by a multitemperature model, and there are different empirical or semiempirical models to calculate nonequilibrium reactions

*macheret@purdue.edu

rates, including Park's model [5], Marrone-Treanor (MT) model [6], and Knab's model [7]. The CFD method with Park's rate model has been calibrated against some experimental data and has successfully reproduced most experimental radiation data available for velocities up to 10 km/s [1,5]. However, the computational cost increases with the number of species, and the method doesn't reveal detailed non-Boltzmann distribution of internal energies, which can be significant at conditions other than those for which the models have been calibrated. The DSMC method [8], which simulates stochastic molecular collisions, overcomes the difficulties of CFD although at a computational cost. Phenomenological models like variable hard sphere (VHS) and variable soft sphere (VSS) [8] are often used to describe collisions. Internal energy exchange and chemical reaction processes occur with a probability depending on the corresponding models. In particular, for the dissociation reaction, there are the total collision energy (TCE) model [8], the vibrational favored dissociation (VFD) model [9], vibrational biased models [10,11], and the quantum kinetics (QK) model [12]. Except the QK model, all other models have calibration constants that are adjusted to reproduce experimentally measured or theoretically calculated nonequilibrium rates. Since the dissociation reaction occurs at high temperature and it is difficult if not impossible to isolate vibrational-vibrational (VV) or vibrational-translational (VT) energy exchange from chemical reactions, direct measurements of nonequilibrium reaction rates are hard to perform. Benefiting from the growth of computational power and improved accuracy of *ab initio* electronic structure calculations, the quasiclassical trajectory (QCT) method enables studies of collisions with high energy and provides detailed state-specific reaction cross sections and rates [13,14]. With the exception of calibrating phenomenological models against QCT data [10,11,15–17], there have been few attempts to use reduced-order models directly in flow simulations [18,19]. However, QCT data are available for only a few simple colliding pairs in their ground electronic states due to the complexity of *ab initio* potential energy surface (PES) calculations. There are also very few independent comparisons of calculations to verify the results and quantify uncertainties. Therefore, models based on simplified but physically justified assumptions are desirable.

In the early 1990s, Macheret *et al.* developed a theoretical model for nonequilibrium dissociation reaction at high-temperature conditions based on the assumption of classical impulsive collisions [20–23]. In the model, the reactive chemical rearrangement in collision is treated as an instantaneous (i.e., impulsive) process that can be described by classical mechanics. Whether the dissociation occurs depends only on the postcollision vibrational energy. It is further assumed that most important features of reaction probabilities and rates are determined by their behavior at or near the energy threshold. With those assumptions, closed-form formulas for the reaction probability were obtained for diatom-atom and diatom-diatom collisions. Integration of the reaction probabilities with the appropriate vibrational and translational energy distribution functions yields, with additional approximations, analytical expressions for the multitemperature dissociation rate coefficients. The multitemperature version of the Macheret-Fridman (MF) model [20–23] has been recently updated and validated against QCT data [24]. DSMC simulations use the reaction probabilities directly, and the MF expression for diatom-atom collisions, with some modifications, has been successfully implemented in DSMC by Boyd [25] as well as Wadsworth and Wysong [26]. DSMC simulations with the model showed a good agreement of the computed mass concentrations with experimental data in the simulation of N_2 and air shocks [25]. However, due to the mathematical approximations, the formula for the reaction probability has singularities for collisions with certain values of energy. The model also yields a reaction probability greater than unity under certain conditions, resulting in the need for a rather artificial cutoff procedure. Moreover, the model for diatom-diatom collisions was not implemented due to the complexity of the formulas.

In this context, the main objective of the work is to eliminate those mathematical approximations in the Macheret-Fridman (MF) model [20–24] that caused singularities and above-unity probabilities. We propose an implementation of the MF model under the DSMC framework. The implementation, called the MF-DSMC model in this paper, follows Macheret *et al.*'s theory of the dissociation reaction, including the assumption of classical impulsive collisions. We assess the model by comparing DSMC calculated reaction rates and chemistry-vibrational energy coupling

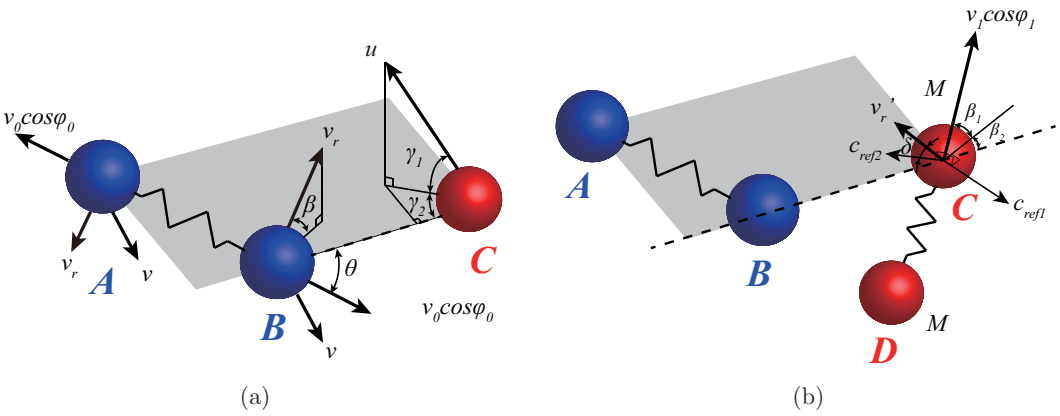

(a) (b)

FIG. 1. Collision geometries: (a) diatom-atom; (b) diatom-diatom.

with recent QCT results and experimental measurements. Physical reasons for the differences between the MF-DSMC and QCT equilibrium reaction rates are discussed, and an approach to remove the differences is developed. As an example, $N_2 + O$ dissociation reaction rates are corrected by using a collision model formulated based on QCT data. The MF-DSMC model is then used to simulate the O_2 shock tube experiments performed by Ibraguimova *et al.* [27].

The rest of this paper is organized as follows. In Sec. II the MF model and the MF-DSMC implementation are introduced. Section III summarizes comparisons of reaction rates and chemistry-vibrational energy coupling between the MF-DSMC model and QCT calculations. Next, the collision model for $N_2 + O$ and the corrected reactions rates based on the MF-DSMC model are presented in Sec. IV. Then the simulations of O_2-reacting shock with the MF-DSMC model are compared with experimental measurements and state-specific calculations in Sec. V. Finally, concluding remarks are given in Sec. VI.

II. MF-DSMC MODEL

The implementation of the MF model under the DSMC framework, i.e., the MF-DSMC model, is based on the original theory proposed by Macheret *et al.* [20–22]. The model is intended for high-temperature or high-energy collisions. At these conditions, the Massey parameter ξ, which is inversely proportional to the velocity of collision, is smaller than one, and thus the collisions are in the impulsive limit [28]. Energy transfer from collisional energy to vibrational energy of the dissociating molecule is determined by the masses of colliding particles and by the set of angles and phases in the instant when the chemical rearrangement occurs. Thus, collision dynamics are weekly sensitive to the details of PES, and the energy transfer can be calculated with the assumption of instantaneous collisions. Detailed derivations of closed-form reaction probabilities and rates can be found in Ref. [20]. For the MF-DSMC model, we make use of the concept of threshold function, which is defined as the minimum collisional (kinetic) energy required for dissociation to occur. In this work, we verify the formulas, rederive the one for the diatom-diatom collision with a different set of coordinates for collision geometries, and extend the model for heteronuclear molecule dissociation.

The collision geometries for diatom-atom and diatom-diatom collisions are shown in Fig. 1. Molecule AB is the dissociating molecule, and CD is the colliding partner. A right-handed coordinate system is defined in a following manner: atoms A, B, and C form the xy plane, and the y axis is in the direction of BC. In the center-of-mass frame, the velocities of molecules AB and BC are v and u accordingly. The angles γ_1 and γ_2 are the polar and azimuthal angles for velocity u. To simplify reaction probability calculations, we assume that the molecular vibrational

motion is harmonic. This means that the phase angles of vibrations φ_0 and φ_1 are distributed uniformly between 0 and 2π, and the maximum velocities of vibrations v_0 and v_1 can be calculated from the corresponding vibrational energy as they would be for a harmonic oscillator. As will be shown in Sec. III A, little error is introduced by the harmonic oscillator assumptions for low-lying vibrational states. For higher vibrational levels, a more precise way of modeling is to first calculate the distribution of the phase angle with the actual potential energy curve and then sample the phase angle based on the distribution [29]. Such anharmonic oscillator modeling would involve considerable additional computational resources and is therefore left for future work.

The magnitudes of vibrational velocities for the specific phase angles are $v_0 \cos\varphi_0$ and $v_1 \cos\varphi_1$. The direction of the AB vibrational velocity is determined by the angle θ. The polar and azimuthal angles of the CD vibrational velocity are β_1 and β_2. v_r is the rotational velocity of molecule AB. Its direction is perpendicular to the vibrational velocity of molecule AB with a polar angle β. To define the direction of rotational velocity v_r' for molecule CD, two reference vectors $\vec{c}_{\text{ref1}}$ and $\vec{c}_{\text{ref2}}$ are introduced. $\vec{c}_{\text{ref1}}$ is in the xy plane and perpendicular to the vibrational velocity v_1. $\vec{c}_{\text{ref2}}$ is perpendicular to both $\vec{c}_{\text{ref2}}$ and v_1. Then the direction of rotational velocity v_r' is uniquely determined by the angle δ between v_r' and $\vec{c}_{\text{ref2}}$, and it must be in the plane formed by $\vec{c}_{\text{ref1}}$ and $\vec{c}_{\text{ref2}}$.

Denote the mass of atoms A, B, C, and D as m_A, m_B, m_C, and m_D, then the reduced mass of molecules AB and BC becomes $\mu_{AB} = m_A m_B/(m_A + m_B)$ and $\mu_{CD} = m_C m_D/(m_C + m_D)$. For the case of the diatom-atom collision, μ_{CD} is equal to the mass of atom C. We can also calculate the reduced mass of the whole system:

$$\mu = \begin{cases} (m_A + m_B)m_C/(m_A + m_B + m_C), & \text{for diatom-atom} \\ (m_A + m_B)(m_C + m_D)/(m_A + m_B + m_C + m_D), & \text{for diatom-diatom} \end{cases}. \tag{1}$$

The relations between velocities and energies become

$$E_v = 2\mu_{AB} v_0^2, \quad E_v' = 2\mu_{CD} v_1^2, \quad E_r = 2\mu_{AB} v_r^2, \quad E_r' = 2\mu_{CD} v_r'^2, \quad E_t = \frac{(m_A + m_B)^2 v^2}{2\mu}, \tag{2}$$

where E_v, E_v' are the vibrational energy of molecules AB and CD, E_r, E_r' are the rotational energy of each molecules and E_t is the collisional energy.

The two-body problem is solved for the elastic collision between atoms B and C. Energy and momentum transfer are allowed only in the direction of collision. By making the postcollision vibrational energy of molecule AB equal to the dissociation energy D, we can obtain the threshold function $F = E_{t,\min}$, which is the minimum collisional energy for the dissociation reaction AB + CD → A + B + CD to occur. For the diatom-atom collision, the threshold function is

$$F = \frac{\mu/\mu_{AB}}{4\cos^2\gamma_1 \cos^2\gamma_2} \left\{ \frac{\sqrt{D - E_v \sin^2\varphi_0} + \sqrt{E_v}\cos\varphi_0}{\cos\theta m_C/(m_B + m_C)} - \frac{2\mu_{AB}}{m_B}[\sqrt{E_v}\cos\varphi_0\cos\theta + \sqrt{E_r}\cos\beta\sin\theta] \right\}^2. \tag{3}$$

For the diatom-diatom collision, the threshold function is

$$F = \frac{\mu/\mu_{AB}}{4\cos^2\gamma_1 \cos^2\gamma_2} \left\{ \frac{\sqrt{D - E_v \sin^2\varphi_0} + \sqrt{E_v}\cos\varphi_0}{\cos\theta m_C/(m_B + m_C)} - \frac{2\mu_{AB}}{m_B}[\sqrt{E_v}\cos\varphi_0\cos\theta + \sqrt{E_r}\cos\beta\sin\theta] - \frac{2\sqrt{\mu_{AB}\mu_{CD}}}{m_C}[\sqrt{E_r'}(\cos\delta\cos\beta_2\sin\beta_1 + \sin\delta\sin\beta_2) - \sqrt{E_v'}\cos\varphi_1\cos\beta_1\cos\beta_2] \right\}^2. \tag{4}$$

The derivations of Eqs. (3) and (4) are based on the assumption that collisions are close to the impulsive limit. It can be found that rotational energy of dissociating molecule E_r contributes to the dissociation by its component along the direction of collision. However, rotational energy also increases the effective dissociation energy due to the centrifugal barrier, which arises as the rotational energy decreases when the molecule is stretched during dissociation. We adopt the strategy proposed in Ref. [20] by using an effective dissociation energy $D_{\rm ef}$, which includes both effects. $D_{\rm ef}$ is evaluated with a long-range potential energy curve $V(r) = -2D(R_{\rm eq}/r)^6$, where $R_{\rm eq}$ is the equilibrium distance of molecular bond and r is the internuclear distance:

$$D_{\rm ef} = D - E_r + \frac{2E_r^{3/2}}{3\sqrt{6D}}. \tag{5}$$

The final expressions of threshold functions for diatom-atom and diatom-diatom collisions are

$$F = \frac{\mu/\mu_{AB}}{4\cos^2\gamma_1\cos^2\gamma_2}\left[\frac{\sqrt{D_{\rm ef} - E_v\sin^2\varphi_0} + \sqrt{E_v}\cos\varphi_0}{\cos\theta m_C/(m_B+m_C)} - \frac{2\mu_{AB}}{m_B}\sqrt{E_v}\cos\varphi_0\cos\theta\right]^2, \tag{6a}$$

$$F = \frac{\mu/\mu_{AB}}{4\cos^2\gamma_1\cos^2\gamma_2}\left\{\frac{\sqrt{D_{\rm ef} - E_v\sin^2\varphi_0} + \sqrt{E_v}\cos\varphi_0}{\cos\theta m_C/(m_B+m_C)} - \frac{2\mu_{AB}}{m_B}\sqrt{E_v}\cos\varphi_0\cos\theta \right.$$
$$\left. - \frac{2\sqrt{\mu_{AB}\mu_{CD}}}{m_C}[\sqrt{E_r'}(\cos\delta\cos\beta_2\sin\beta_1 + \sin\delta\sin\beta_2) - \sqrt{E_v'}\cos\varphi_1\cos\beta_1\cos\beta_2]\right\}^2. \tag{6b}$$

It should be noted that, for a diatom-diatom colliding pair like $O_2 + N_2$, there is more than one possible dissociation reaction channel. With the same definitions of generalized coordinates in Fig. 1, we derive the threshold function for the dissociation of the CD molecule as well, which is shown as

$$F' = \frac{\mu/\mu_{CD}}{4\cos^2\gamma_1\cos^2\gamma_2}\left\{\frac{\sqrt{D'_{\rm ef} - E'_v\sin^2\varphi_1} + \sqrt{E'_v}\cos\varphi_1}{\cos\beta_1\cos\beta_2 m_B/(m_B+m_C)} - \frac{2\mu_{CD}}{m_C}\sqrt{E'_v}\cos\varphi_1\cos\beta_1\cos\beta_2\right.$$
$$\left. + \frac{2\sqrt{\mu_{AB}\mu_{CD}}}{m_B}[\sqrt{E_r}\cos\beta\sin\theta + \sqrt{E_v}\cos\varphi_0\cos\theta]\right\}^2. \tag{7}$$

With the complete descriptions of threshold functions, the MF-DSMC model can be formulated. As mentioned in Sec. I, the MF model calculates reaction probabilities $P(E_t)$ by expanding Eqs. (6a) and (6b), and (7) in the Taylor series of phase angles and calculating the probability of $E_t \geqslant F$. The mathematical approximation introduced by the Taylor expansion results in singularities of reaction probabilities. Here, instead of using the Taylor expansion, we use a different technique. Because DSMC is a stochastic method and the collision model doesn't change the distributions of phase angles, we can directly sample collision geometries and use the threshold function to determine whether dissociation occurs. The ensemble average will then produce the correct reaction probabilities. The pseudocodes are listed in Algorithm 1.

It should be noted that $D_{\rm ef}$ and the term $D_{\rm ef} - E_v\sin^2\varphi_0$ in Eqs. (6a) and (6b) and (7) may become less than 0 for certain values of energies of the colliding particles. This is due to the particular form of the potential energy curve used to derive $D_{\rm ef}$. We have used a more realistic potential energy curve, the Morse potential, to remove this singularity but found that the change in final results is not significant. Thus, a simple recipe is to make the reaction probability P equal to 1 when this condition occurs.

Algorithm 1: MF-DSMC Model

1: Generate phase angles γ_1, γ_2, β_1, β_2, θ, φ_0, φ_1, θ, δ, β;
2: Compute effective dissociation energy $D_{\mathrm{ef},i}$ with Eq. (5);
3: Compute threshold energy $F_i(E_v, E_r, E'_v, E'_r)$ with Eqs. (6a), (6b) and (7) for each possible dissociation reaction channel i;
4: Select the reaction pathway i with the minimum threshold energy F_i;
5: **if** $\boldsymbol{E}_t \geqslant \boldsymbol{F}_i$ **then** Reaction i occurs (i.e.,$P_{j=i} = 1$, $P_{j\neq i} = 0$);
6: **else** No dissociation occurs (i.e., $P_j = 0$);
7: **end if**

III. VALIDATION OF THE MODEL

To validate the MF-DSMC model, we implemented the model in a heavily modified DS1V code [8]. A standard no-time-counter (NTC) scheme is used. Elastic collisions are modeled according to the variable hard sphere (VHS) model [8]. The reference diameter d_{ref} and viscosity index ω for different species are listed in Table I. The VHS parameters for O_2-O_2, O_2-N_2, and NO-N_2 are calculated using collisional integrals for high-temperature air species [30]. Regarding modeling of internal energy, a discrete vibrational energy model is used with continuous model for rotational energy. The vibrational ladders calculated in Refs. [31,32] are used in this work. All the calculations are started at either thermal equilibrium ($T = T_r = T_v$) or nonequilibrium ($T = T_r \neq T_v$) conditions with Maxwell-Boltzmann distribution of collisional energy and internal energy. In order to isolate the influence of reaction models from the VT and RT energy relaxations, the Larsen-Borgnakke (LB) model with constant $Z_R = 1$ and $Z_V = 10^4$ is used. To maintain the steady state and isothermal condition, dissociations are only tracked, and molecules are not actually dissociated.

A very important feature of the MF model is that it calculates the probability of the dissociation reaction provided that a collision occurs. Therefore, in order to calculate the total probability and rate of dissociation, one needs to multiply the MF probability by the rate of collisions, which has to be taken from outside the MF model. For example, the rate of collisions can be calculated with the VHS model or from matching the thermal equilibrium rate to the experimental or QCT data. In this context, we first validate the MF-DSMC model by comparing the nonequilibrium characteristics such as state-specific rates and nonequilibrium factors to the available data, and then examine the absolute dissociation rates that require knowledge of the collision rates.

A. Vibrational state-specific rates

Vibrational state-specific reaction rates for different colliding pairs are compared in Fig. 2. We assume that translational and rotational mode are in thermal equilibrium (i.e., $T = T_r$), then the rates can be calculated as

$$k(T, E_v) = \frac{\sum_{J=0}^{J_{\max}(v)} k(T, v, J) n_J \exp[-E_{rv}(v, J)/k_B T]}{\sum_{J=0}^{J_{\max}(v)} n_J \exp[-E_{rv}(v, J)/k_B T]}, \tag{8}$$

where $k(T, v, J)$ is the QCT calculated rovibrational state-specific reaction rates, n_J is the product of nuclear spin and rotational degeneracy, $J_{\max}(v)$ is the maximum rotational quantum number for

TABLE I. VHS parameters with $T_{\mathrm{ref}} = 273$ K.

Colliding pair	N_2-N [33]	O_2-O [34]	N_2-O [33]	N_2-N_2 [33]	O_2-O_2	O_2-N_2	NO-N_2
d_{ref} (Å)	3.585	3.442	3.814	4.170	4.152	4.051	4.341
ω	0.770	0.750	0.750	0.740	0.732	0.734	0.729

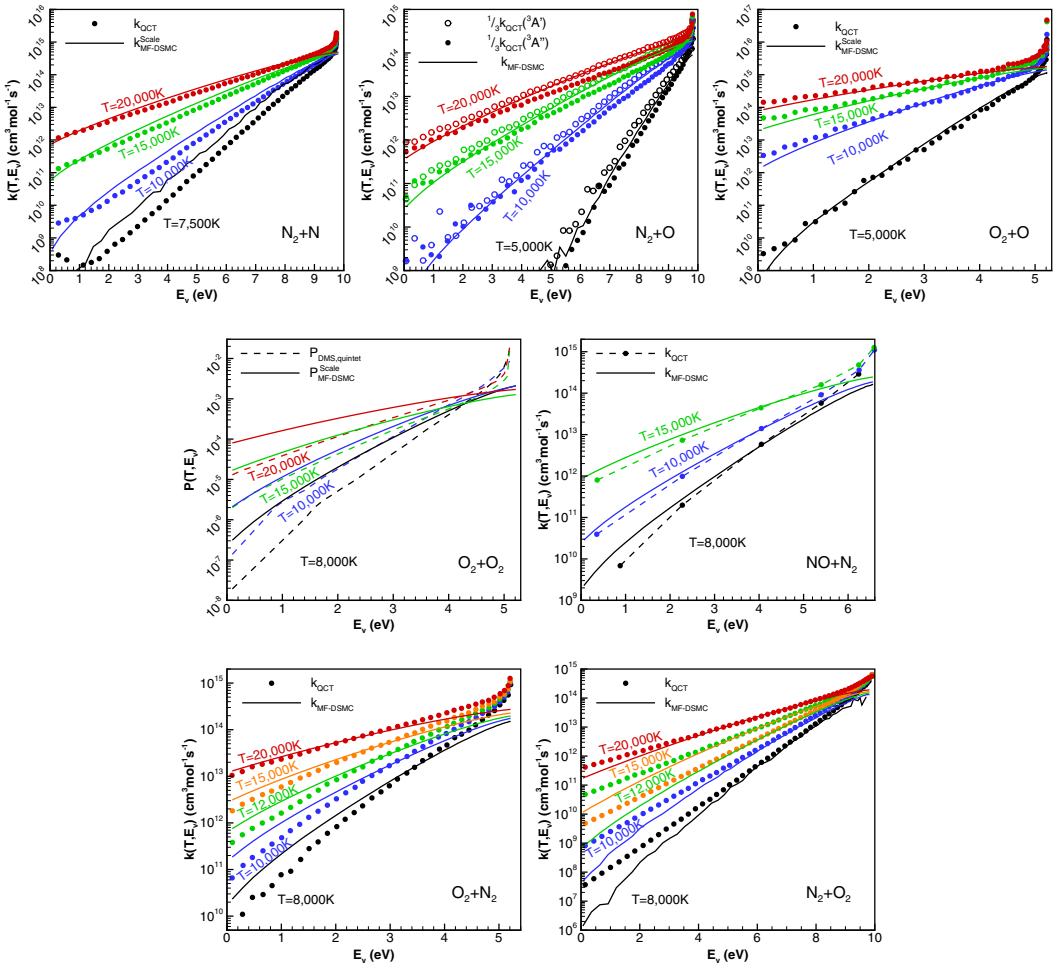

FIG. 2. Comparison of vibrational state-specific rates calculated by the QCT method and MF-DSMC model. MF-DSMC rates for $N_2 + N$, $O_2 + O$, and $O_2 + O_2$ are scaled.

vibrational state v, and E_{rv} is the coupled rovibrational energy. Equation (8) is used to calculate $k(T, E_v)$ for $N_2 + N$ [35], $N_2 + O$ [32], and $O_2 + O$ [19] systems. For NO dissociated by N, N_2 dissociated by O_2 and O_2, dissociated by N_2, the rates are directly obtained from Refs. [36,37]. It should be noted that ground state $N_2(X^1\Sigma_g^+)$ and $O(^3P)$ correlate with three electronic states of N_2O, but only two of them, $^3A''$ and $^3A'$, correlate with ground state atomic nitrogen in the dissociation reaction channel. For Fig. 2, we take the QCT results for both PESs and multiply the rates by the weight of each PES. To remove the effect of collision rates and to focus on the MF-DSMC model itself, DSMC calculated rates are scaled as

$$k^{\text{Scale}}_{\text{MF-DSMC}}(T, E_v) = k_{\text{MF-DSMC}}(T, E_v)\frac{k_{\text{eq,QCT}}(T)}{k_{\text{eq,MF-DSMC}}(T)}, \tag{9}$$

where $k_{\text{eq,QCT}}$ and $k_{\text{eq,MF-DSMC}}$ are the corresponding equilibrium dissociation rates predicted by the QCT method and MF-DSMC model. For O_2 dissociated by O_2, there are DMS calculated probabilities of dissociation $P_{DMS}(T, E_v)$ [38], but the collision rates are unknown. Since the

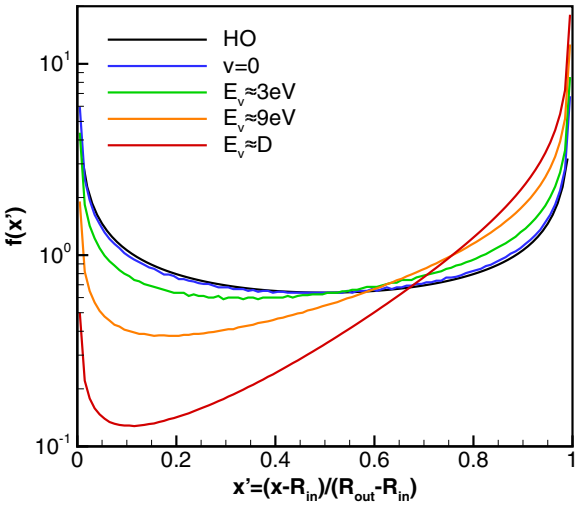

FIG. 3. Probability density functions of internuclear distance for the N_2 molecule at different values of vibrational energy.

collision rate $k_{\text{coll}}(T)$ is independent of vibrational level, we have

$$\frac{k(T, E_v)}{k_{\text{eq}}(T)} = \frac{k_{\text{coll}}(T)P(T, E_v)}{\sum_{v=0}^{v=v_{\max}} k_{\text{coll}}(T)P(T, E_v)\exp(-E_v/k_BT)} = \frac{P(T, E_v)}{\sum_{v=0}^{v=v_{\max}} P(T, E_v)\exp(-E_v/k_BT)}. \tag{10}$$

Therefore, we compare the following scaled probability of reaction for the $O_2 + O_2$ system with the DMS calculated values:

$$P^{\text{Scale}}_{\text{MF-DSMC}}(T, E_v) = P_{\text{MF-DSMC}}(T, E_v)\frac{\sum_{v=0}^{v=v_{\max}} P_{DMS}(T, E_v)\exp(-E_v/k_BT)}{\sum_{v=0}^{v=v_{\max}} P_{\text{MF-DSMC}}(T, E_v)\exp(-E_v/k_BT)}. \tag{11}$$

As seen in Fig. 2, there is a good agreement of MF-DSMC vibrational state-specific reaction rates with QCT and DMS ones for most systems investigated here. The MF-DSMC model correctly captures the linear dependence of $\log(k(T, E_v))$ on vibrational energy and also the relationship between the slope of the logarithm of the rates and translational temperature T. For the $N_2 + O$ system, the model predicts rates almost identical to the QCT results multiplied by the electronic degeneracy factor. The agreement improves with increasing temperature, which confirms the expectation that collision dynamics are weakly sensitive to the details of PES at high-temperature and high-energy collisions. The model fails to correctly predict the nonlinear part of vibrational state-specific rates for very high vibrational states because it assumes harmonic vibrations. The probability density functions of normalized internuclear distance for the N_2 molecule with different values of vibrational energy are compared in Fig. 3. Compared to the harmonic oscillator (HO), the actual particles spend more time at the outer turning point, which is the preferential phase angle for dissociation [20]. Thus, the HO assumption results in underestimation of the dissociation rates and probabilities for molecules with high vibrational energy. The issue becomes less significant for either high translational temperature or low vibrational temperature because of the increasing contributions from molecules with low vibrational energy.

B. Nonequilibrium factors

Although not directly used in DSMC, multitemperature reaction rates are crucial in nonequilibrium CFD simulations. For flow conditions like shock wave or expansion fan, strong deviations

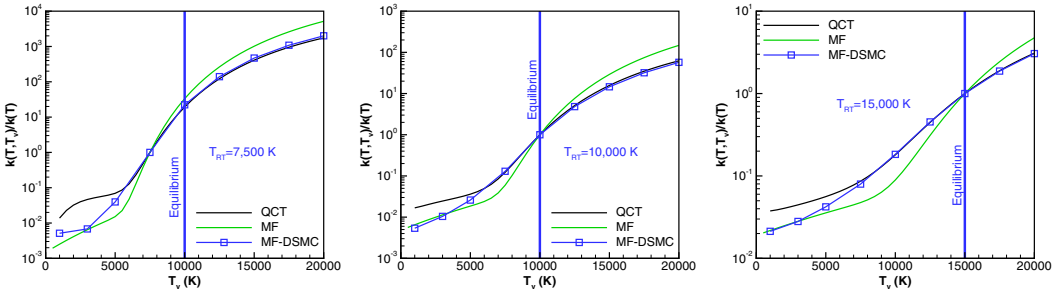

FIG. 4. Nonequilibrium factor for $N_2 + N \rightarrow N + N + N$.

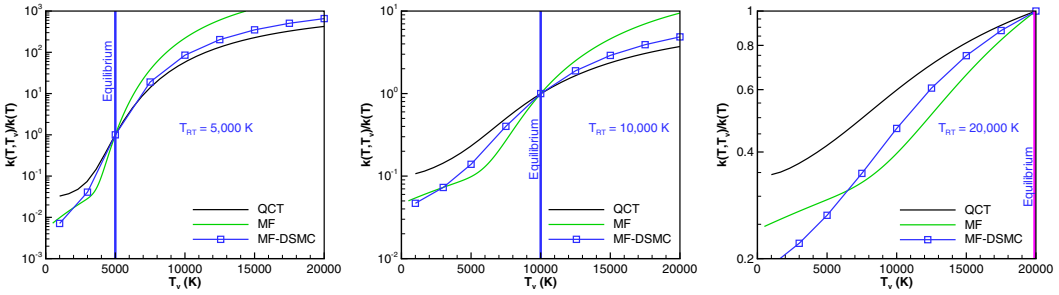

FIG. 5. Nonequilibrium factor for $O_2 + O \rightarrow O + O + O$.

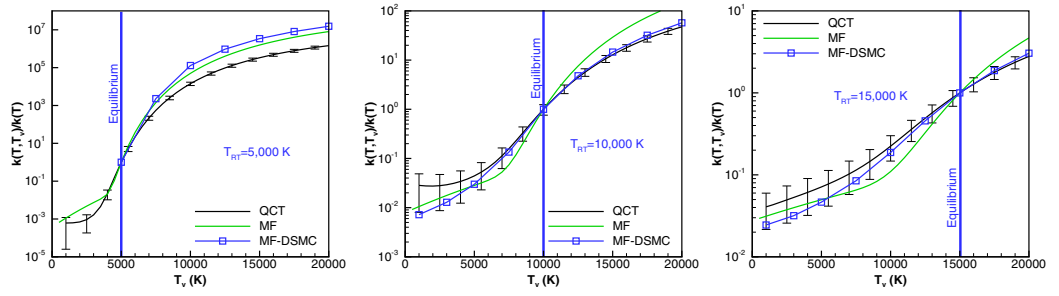

FIG. 6. Nonequilibrium factor for $N_2 + O \rightarrow N + N + O$.

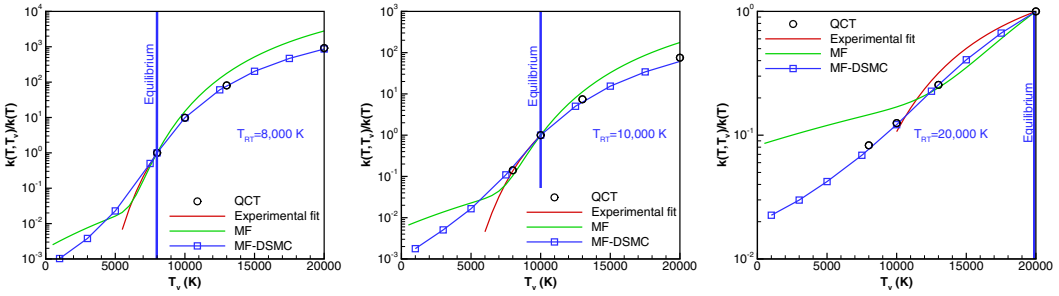

FIG. 7. Nonequilibrium factor for $N_2 + N_2 \rightarrow N + N + N_2$.

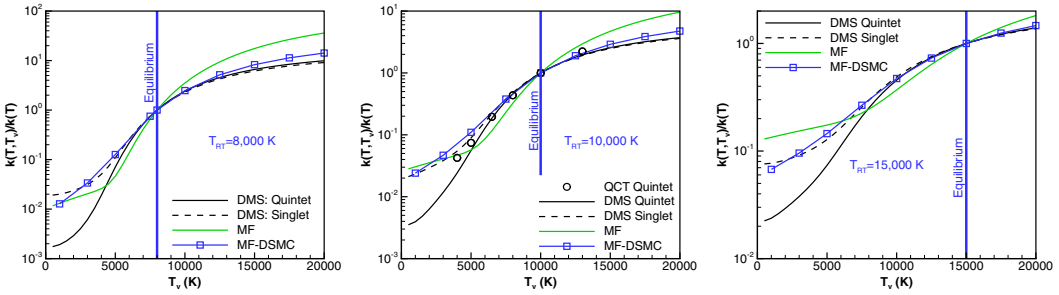

FIG. 8. Nonequilibrium factor for $O_2 + O_2 \rightarrow O + O + O_2$.

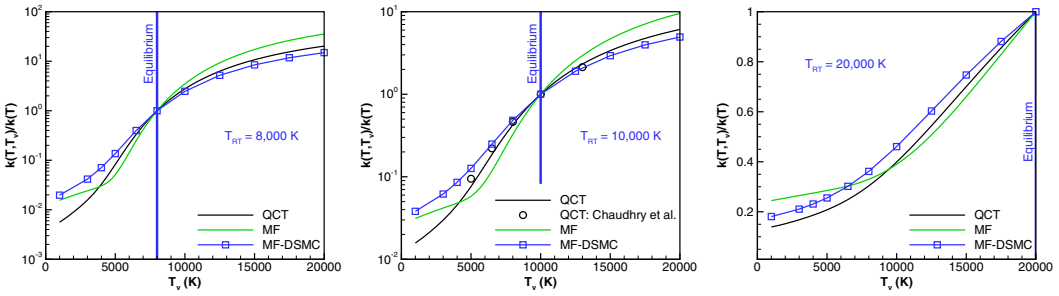

FIG. 9. Nonequilibrium factor for $O_2 + N_2 \rightarrow O + O + N_2$.

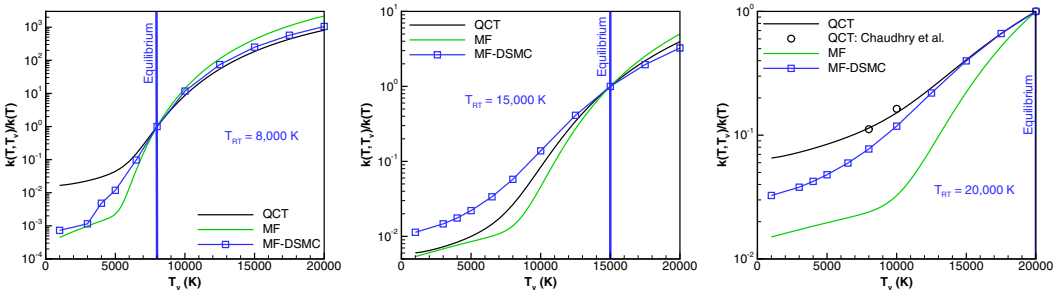

FIG. 10. Nonequilibrium factor for $N_2 + O_2 \rightarrow N + N + O_2$.

from thermal equilibrium result in several orders of magnitude difference in reaction rates and heat transfer. Comparison of nonequilibrium two-temperature reaction rates generated with MF-DSMC to those calculated by QCT or obtained from experiments can help evaluate the model consistently.

To remove the influence of collisional model, we compare nonequilibrium factor Z defined as the ratio of two-temperature rates $k(T, T_v)$ and the corresponding equilibrium rates $k_{\text{eq}}(T)$ in this work. There are few experimental measurements of the value. Losev *et al.*'s fit [39] of their experimentally measured N_2 dissociation rates [40] is the only one included here. For other systems, the nonequilibrium reaction rates are calculated from QCT data. For $N_2 + N$ [35], $N_2 + O$ [32], and $O_2 + O$ [19], the two-temperature rates are calculated from rovibrational state-specific dissociation rates with a fully coupled rovibrational ladder:

$$k(T, T_v) = \frac{\sum_{v,J} n_J k(T, v, J) \exp\left[-\frac{E_v(v)}{k_B T_v}\right] \exp\left[-\frac{E_{rv}(v,J)-E_v(v)}{k_B T}\right]}{\sum_{v,J} n_J \exp\left[-\frac{E_v(v)}{k_B T_v}\right] \exp\left[-\frac{E_{rv}(v,J)-E_v(v)}{k_B T}\right]}. \tag{12}$$

For $O_2 + N_2$ [37] and $N_2 + O_2$ [37], the rates are calculated from vibrational state-specific rates:

$$k(T, T_v) = \frac{\sum_v k(T, v) \exp[-E_v(v)/k_B T_v]}{\sum_v \exp[-E_v(v)/k_B T_v]}. \tag{13}$$

For $O_2 + O_2$ [38], the nonequilibrium factor is directly calculated from the probability of reaction $P(T, E_v)$ as

$$Z(T, T_v) = \frac{\sum_v P(T, E_v) \exp(-E_v/k_B T_v)}{\sum_v P(T, E_v) \exp(-E_v/k_B T)}. \tag{14}$$

Chaudhry and Bender reported two-temperature rates of $N_2 + N_2$ [41] and $N_2 + O_2$ [42,43] systems for specific temperatures. Their results are shown as discrete symbols in the comparisons. In addition, the nonequilibrium factor calculated analytically from the MF model including the vibrational-rotational effect [20,24] are also compared here.

The comparison of nonequilibrium factors is shown in Figs. 4–10. Overall, the results predicted with the MF-DSMC model and QCT calculations match closely. Compared to the original two-temperature MF model, the agreement is especially better at vibrationally hot conditions. The difference between the MF-DSMC model and QCT data is negligible for the $N_2 + N$ and $N_2 + N_2$ systems. For the vibrationally cold condition, the nonequilibrium factor calculated from the MF-DSMC model agrees with QCT data quite well, especially considering the uncertainty of QCT calculations (with the error bars illustrated in Fig. 6). For a weakly nonequilibrium condition with $|T - T_v|/T \leqslant 20\%$, the differences are within a factor 2 for most systems investigated here.

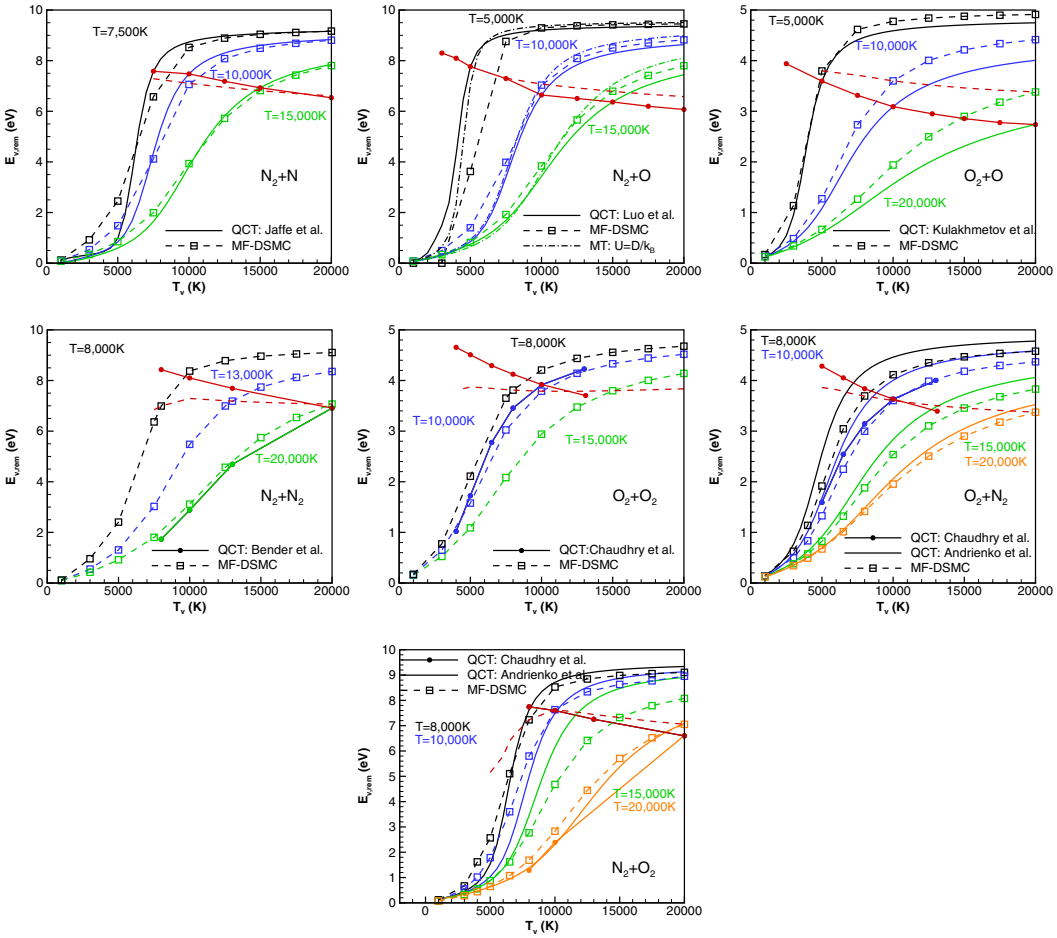

FIG. 11. Comparison of the average vibrational energy removed by dissociation reactions. Red lines for thermal equilibrium conditions $T = T_v$; other lines for vibrational nonequilibrium conditions $T \neq T_v$.

C. Vibrational energy consumption in dissociation

In thermochemical nonequilibrium, the vibrational and rotational energy consumption in the dissociation represents an important part of the overall relaxation process, which, in turn, affects the reaction itself. In a state-specific chemical reaction model or particle-based simulation method, the vibrational and rotational energy consumption is naturally accounted for. However, for CFD with a multitemperature model, bulk chemical species with Boltzmann distributions of internal states are assumed, and the vibrational or rotational energy consumption must be explicitly modeled. In this section, we compare the average vibrational energy removed by dissociation reactions (i.e., $E_{v,\mathrm{rem}}$) in order to validate MF-DSMC model and to provide informations for CFD modeling of thermal nonequilibrium chemical reactions. The baseline values of $E_{v,\mathrm{rem}}$ are calculated from vibrational state-specific rates obtained by the QCT method,

$$E_{v,\mathrm{rem}}(T, T_v) = \frac{\sum_v E_v(v) k(T, v) x(T_v, v)}{\sum_v k(T, v) x(T_v, v)}, \tag{15}$$

where $E_v(v)$ is the vibrational energy of vibrational state v and $x(T_v, v)$ is the corresponding mole fraction for the given vibrational temperature T_v. For the DSMC method, $E_{v,\mathrm{rem}}$ are calculated

implicitly as

$$E_{v,\mathrm{rem}}(T, T_v) = \frac{1}{N_{\mathrm{diss}}} \sum_{i}^{N_{\mathrm{diss}}} E_v(i), \tag{16}$$

where $E_v(i)$ is the vibrational energy of molecule i that dissociates and N_{diss} is the total number of molecules that dissociate.

The comparison is shown in Fig. 11. Red lines denote the average vibrational energy removed at thermal equilibrium conditions, and the other lines represent the values at nonequilibrium conditions. It is seen that the MF-DSMC model reproduces $E_{v,\mathrm{rem}}$ within 15% error for most dissociation reactions. The biggest difference is at low translational temperature since the probabilities of reactions are too low for the DSMC method to resolve the accurate value of $E_{v,\mathrm{rem}}$. For O_2 dissociated in collisions with N_2, there is some disagreement between the two sets of QCT data as T_v increases. The MF-DSMC model underpredicts $E_{v,\mathrm{rem}}$ by up to 0.2 eV at vibrationally cold conditions and agrees well with Chaudhry *et al.*'s results at vibrationally hot conditions. The model overpredicts $E_{v,\mathrm{rem}}$ for O_2 dissociation in collisions with atomic oxygen. The reason for this is unclear. One of the plots in Fig. 11, the one for $N_2 + O$, also shows the $E_{v,\mathrm{rem}}$ calculated with the empirical Marrone-Treanor (MT) model [6]. Although not shown here, the nonpreferential dissociation model that equates $E_{v,\mathrm{rem}}$ to the average vibrational energy at vibrational temperature T_v would strongly disagree with both MF-DSMC and QCT. As seen in Fig. 11, $E_{v,\mathrm{rem}}$ has strong dependence on translational temperature. As translational temperature increases, more molecules with low vibrational energy will have enough total energy to overcome the reaction barrier and dissociate. Hence, $E_{v,\mathrm{rem}}$ should decrease with increasing translational temperature if the vibrational temperature is fixed. Preferential dissociation models such as MT model [6] can perform quite well as seen in Fig. 11 for N_2 dissociation in collisions with atomic oxygen.

D. Equilibrium dissociation rates

We now compare the calculated equilibrium dissociation rates with recent theoretical calculations [19,31,32,35–38,41–47], experimental measurements [27,48–53], and empirical estimations [5,54–57]. The QCT data used here include Esposito *et al.*'s [44] and Jaffe *et al.*'s [35] calculations of $N_2 + N$, Andrienko *et al.*'s [45], Esposito *et al.*'s [31], and Kulakmetov *et al.*'s [19] calculations of $O_2 + O$, Esposito *et al.*'s [46] and Luo *et al.*'s [32] calculations of $N_2 + O$, Bender *et al*'s [41] calculations of $N_2 + N_2$, Andrienko *et al.*'s [37] and Chaudhry *et al.*'s [42] calculations of $O_2 + N_2$, and Andrienko *et al.*'s [36] calculations of NO+N_2. For the ground state $O_2(X^3\Sigma_g^-)$, there are three spin states, singlet, triplet, and quintet, for the O_2-O_2 dimer. There are no complete QCT calculations for all these states. Besides, there is more than one possible electronic state to have the dissociation reaction. Andrienko *et al.* [47] and Chaudhry *et al.* [43] calculated thermal equilibrium dissociation rates individually with the QCT method using an empirical O_4 PES and an *ab initio* PES. Without a factor that reflects the degeneracy of electronic state ($\eta = 16/3$), Andirenko *et al.*'s rates agree well with Byron [51] and Ibraguimova *et al.*'s measurements [27] for $T < 6000$ K, and Chaudhry *et al.*'s rates show better agreement for $T > 6000$ K. Grover *et al.* [38] performed direct molecular simulation (DMS) with the *ab initio* PES and obtained nonequilibrium dissociation rates with T_v lower than T by around 2000 K.

The computed thermal equilibrium dissociation rates are compared to the experimental data and rates recommended based on experimental data, as well as to the QCT sets discussed in Figs. 12 and 13. It is seen that the rates calculated with the MF-DSMC model are lower than the QCT data by an approximately constant factor. This is especially the case for N_2 dissociation. It is interesting to note that the equilibrium dissociation rates predicted by the MF-DSMC model for $N_2 + N_2$ show good agreements with QCT data. The agreement for $N_2 + O_2$ is also good for $T \geqslant 10\,000$ K, but the rates are lower than Wray *et al.*'s estimation [57] by more than an order of magnitude for lower temperatures.

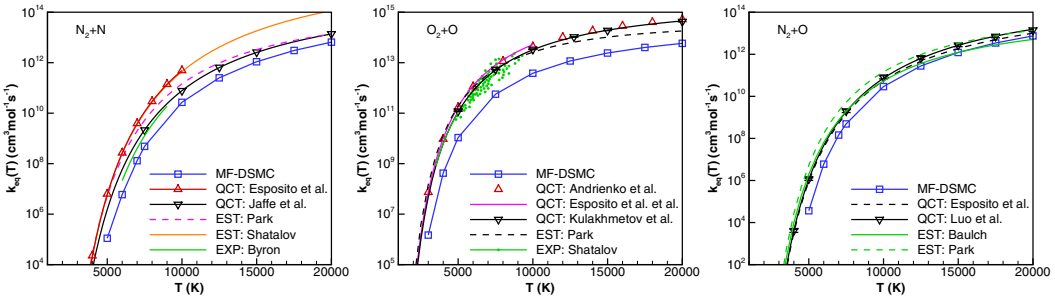

FIG. 12. Comparison of diatom-atom equilibrium dissociation rates. The MF-DSMC rates were calculated with VHS collision rates.

Since the nonequilibrium factors calculated with the MF-DSMC model were found in Sec. III B to agree very well with QCT data, the disagreement between the calculated equilibrium rates and the QCT data is clearly due to the underestimation of total collision cross sections and rates by the

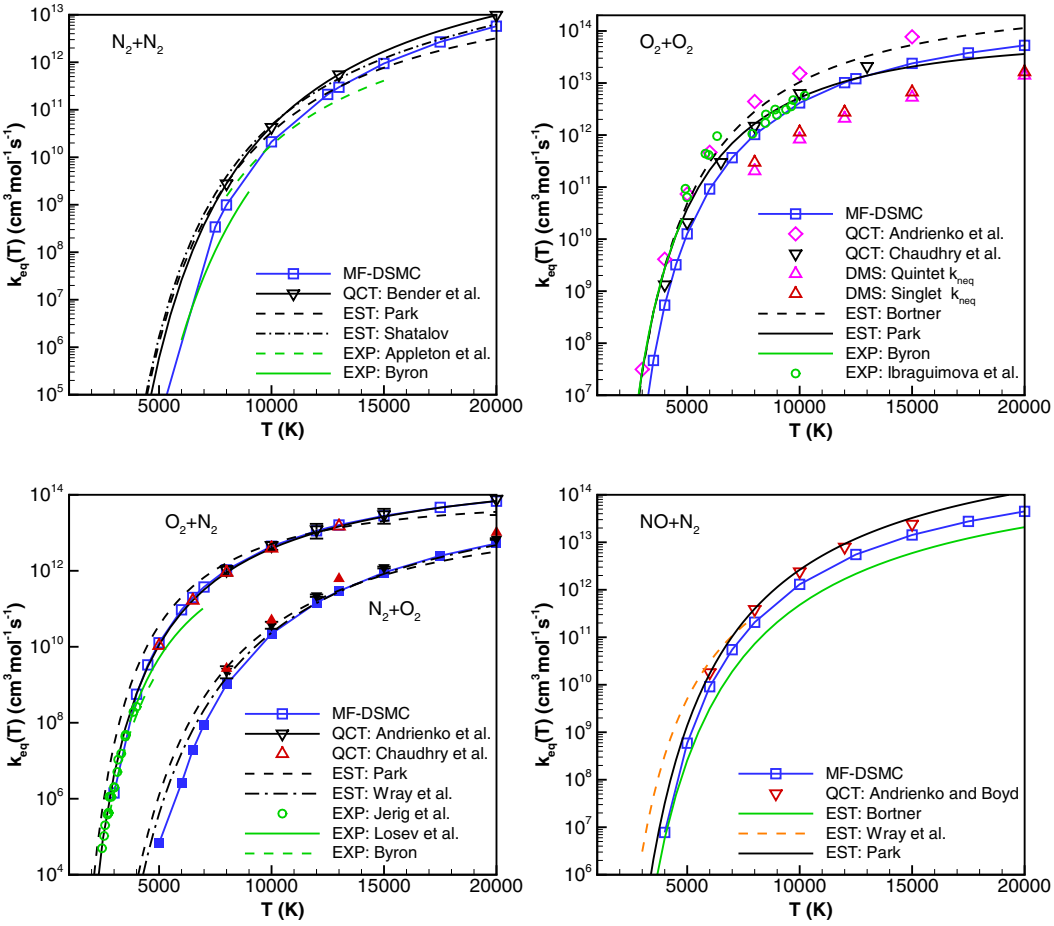

FIG. 13. Comparison of diatom-diatom equilibrium dissociation rates. The MF-DSMC rates were calculated with VHS collision rates. QCT and DMS calculated rates for $O_2 + O_2$ are not multiplied by the electronic degeneracy factor $\eta = 16/3$.

VHS model commonly used in DSMC rather than to the MF dissociation model itself. Therefore, to improve the model, MF-DSMC should be paired with a better collision model. The details will be discussed in Sec. IV.

IV. QCT-BASED COLLISION MODEL

As stated in Sec. III, the difference between the thermal equilibrium dissociation rates computed with MF-DSMC and QCT is a result of different collision models rather than of MF theory. Indeed, the MF theory described in Sec. II deals with energy transfer during chemical rearrangement assuming that the collision did happen. The reaction probability is the product of two probabilities: the probability of collision and the probability that dissociation occurs in the collision. It is the latter probability that is calculated in the MF theory, while the probability of collision has to be determined separately. The nonequilibrium factors, i.e., the nonequilibrium rates normalized by thermal equilibrium rates, as well as the mean vibrational energy removed in dissociation, do not depend on the collision model, and here, as seen in Sec. III A, III B, and III C, MF-DSMC performs quite well. On the other hand, the absolute rates computed with MF-DSMC (Sec. III D) are lower than those calculated with QCT by a nearly constant factor. Thus, in order to improve the model, the collision model has to be improved.

Since the VHS model was first proposed more than 30 years ago by Bird [8], it is still one of the most widely used collision models for DSMC. The model is convenient due to its simple mathematical form and the model parameters can be calibrated to reproduce experimentally measured or calculated viscosities and thermal conductivities. However, the VHS model is problematic when the temperature deviates substantially from the reference temperature [58]. The model assumes an isotropic scattering law, which was subsequently improved in the variable soft sphere (VSS) model [59] with an additional parameter. The additional parameter changes the most probable scattering angle to a value less than 90° and provides better agreement of multispecies diffusivity with experiments. However, recent QCT calculations [60] have found that the model still overpredicts the scattering angle, especially at hyperthermal conditions. The larger scattering angle results in more efficient transport of mass, momentum, and energy. Therefore, in order to reproduce correct transport coefficients, the model uses smaller total cross sections than the actual ones. This has been found in Ref. [61] for $N_2 + N$ collisions and will be shown below for $N_2 + O$ collisions. Additionally, the purely repulsive hard-sphere potential assumed by the VHS model is inaccurate for both low [58] and high (>1 eV) [62] temperatures. For the former case, the long-range attractive force is dominant, and the Lennard-Jones potential works better. For the latter case, the colliding pair

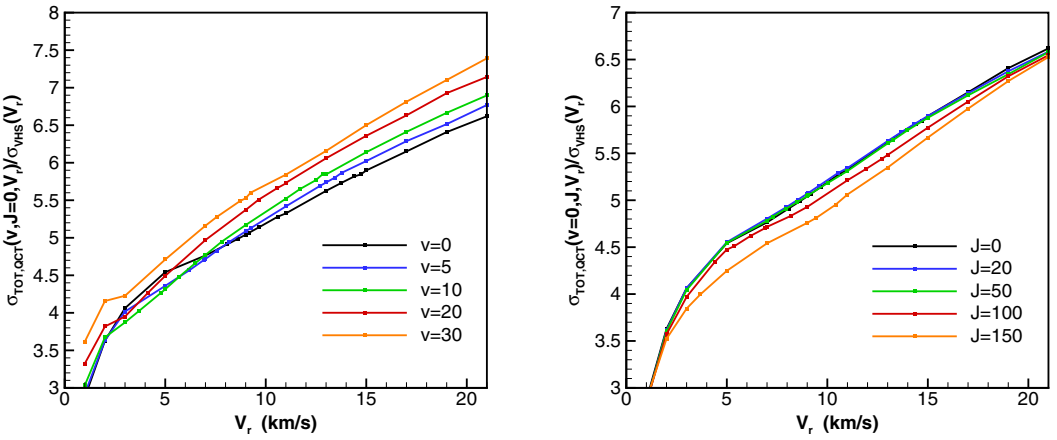

FIG. 14. Comparison of QCT calculated total cross sections for different vibrational states and rotational states.

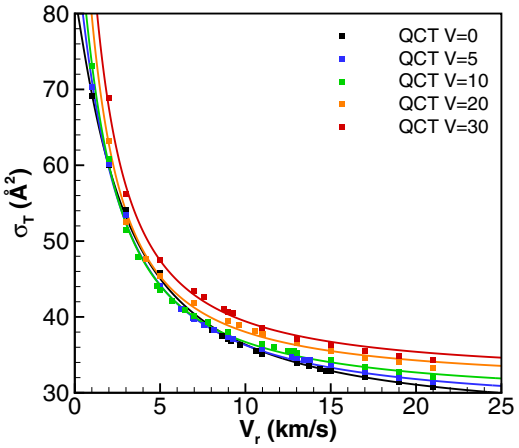

FIG. 15. Comparison of fitted total cross sections and QCT data.

can reach shorter internuclear distances, and an exponential repulsive potential is more physically realistic.

To improve the modeling of collisions in DSMC, we first calculate the total cross sections defined from QCT data for $N_2 + O$ collisions as

$$\sigma_{T,\,\mathrm{QCT}} = \sigma_{\mathrm{elastic}}(\chi > 1^\circ) + \sigma_{\mathrm{inelastic}} + \sigma_{\mathrm{reaction}}, \tag{17}$$

where $\sigma_{\mathrm{elastic}}(\chi > 1^\circ)$ are the elastic collision cross sections with the scattering angle χ larger than one degree, $\sigma_{\mathrm{inelastic}}$ are the inelastic cross sections for collisions with at least one quantum change of vibrational or rotational energy, and $\sigma_{\mathrm{reaction}}$ are the reaction cross sections. The total cross sections normalized by VHS cross sections are shown in Fig. 14. It is seen that the VHS model significantly underpredicts the total cross sections. QCT total cross sections are at least a factor of three larger than VHS cross sections. The total cross section changes slightly with increasing rotational level. Importantly, it increases considerably with the vibrational level of the N_2 molecule because of the larger internuclear distance. We fit the vibrational state-specific total cross sections with the

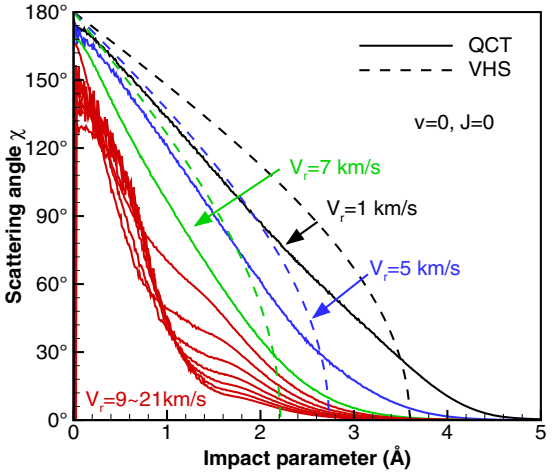

FIG. 16. Comparison of QCT scattering law for N_2 ($v = 0$, $J = 0$) and the VHS model.

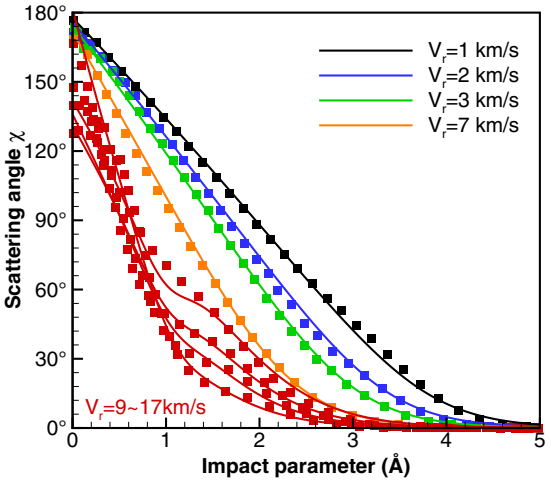

FIG. 17. Comparison of fitted scattering law and QCT data.

following analytical function:

$$\sigma_T = \sigma_0 \exp\left(a E_v + \left(b_1 + b_2 E_v^2\right) \tanh\left\{c\left[\log E_t - \left(d_1 E_{v^2} + d_2 E_v + d_3\right)\right]\right\}\right),$$
$$\sigma_0 = 69.0592\,\text{Å}^2,\ a = 0.0510044,\ b_1 = -0.584551,$$
$$b_2 = -2.96928 \times 10^{-3},\ c = 0.281619,\ d_1 = 0.0301812,\ d_2 = -0.436593,\ d_3 = 0.152225, \tag{18}$$

where E_v and E_t are the vibrational and translational energy in electron-volts and σ_T is the total cross sections in Å^2. The fitting is shown in Fig. 15. The maximum fitting error is less than 1 Å^2.

To ensure correct transport coefficients, average scattering angles of nonreactive collisions are calculated for N_2 with ground rovibrational level. The scattering law is compared to the VHS model in Fig. 16. As discussed above, the VHS model overpredicts the scattering angle. The linear dependence of scattering angles on impact parameters is not captured by the VHS model. Besides,

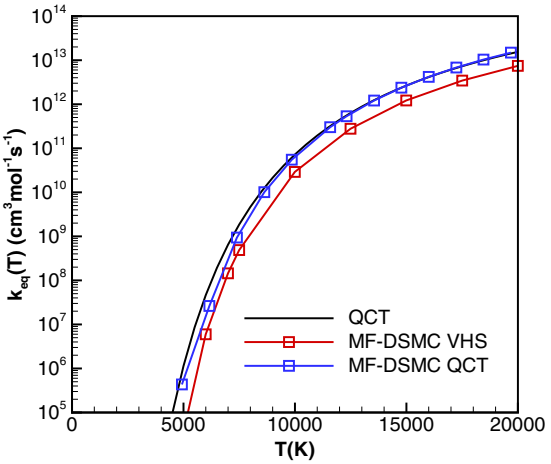

FIG. 18. Comparison of equilibrium dissociation rates for N_2 dissociation in collisions with atomic oxygen.

TABLE II. Free-stream conditions of O_2-reacting shock.

Mach number	Pressure (Torr)	Shock speed (km/s)	Temperature (K)
9.3	2.0	3.07	295
13.4	0.8	4.44	295

the average scattering angle for head-on collisions is not 180° at hyperthermal conditions. Bimodal behavior is found here. Such a feature cannot be predicted by existing phenomenological models. The QCT scattering law was fitted by an analytical function, and the fitting results are shown in Fig. 17. The maximum deviation is less than 10°.

The QCT-based collision model was implemented in DS1V code [8]. Equilibrium dissociation rates calculated from the MF-DSMC model with the VHS collision model and QCT-based collision model are compared in Fig. 18. Better agreement with QCT data is obtained. For $T > 10\,000$ K, the difference between MF-DSMC and QCT is negligible, which justifies the assumption of an impulsive limit for high-energy collisions and dissociation reactions. For other colliding partners, similar procedures of correcting total collision cross sections and scattering law can be used. It should be noted that, since the collision rates are changed by the collision model, vibrational and rotational relaxation numbers should also be calibrated consistently in order to reproduce the correct relaxation times.

V. DSMC SIMULATIONS OF O_2-REACTING SHOCK

In this section, we evaluate the MF-DSMC model by simulating O_2-reacting shock experiments by Ibraguimova *et al.* [27]. The case has been extensively used to validate nonequilibrium chemical reaction models. Studies using QCT based state-specific rates [63] or cross sections [64] in general show good agreement for flow properties. Additionally, adjusting empirical vibrational-favoring models such as the Marrone-Treanor model [65] and Kuznestsov state-specific model [27,34] to match QCT data produces better agreement with the shock tube experiments than the original Marrone-Treanor and Kuznestsov models.

In the present work, two different free-stream conditions are considered, listed in Table II. The DSMC code used to calculate reaction rates in Sec. III is employed to simulate the one-dimensional flow. The collision procedure is summarized in Fig. 19. Main changes include the implementation of carefully tuned total collision cross sections σ_T and the change of scattering procedure, which are enclosed by dashed lines in the figure. The implementation of scattering procedure is aimed at reproducing transport properties. The total cross sections are modeled with the calibrated-VHS model (cVHS), which uses the mathematical form of the VHS model but has different parameters. These parameters are optimized in order to reproduce correct equilibrium

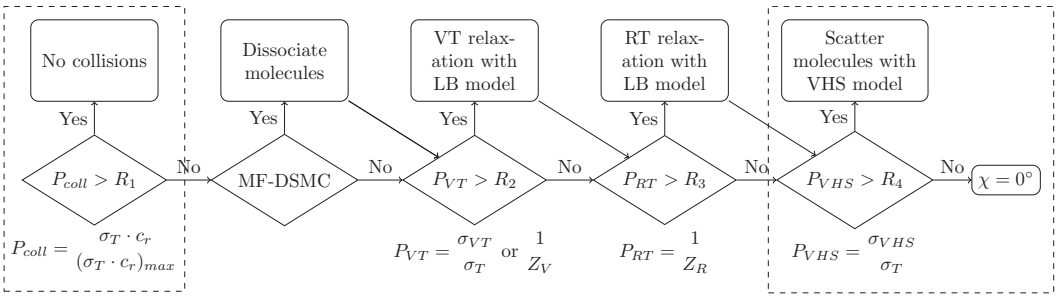

FIG. 19. Collision procedure of the DSMC code.

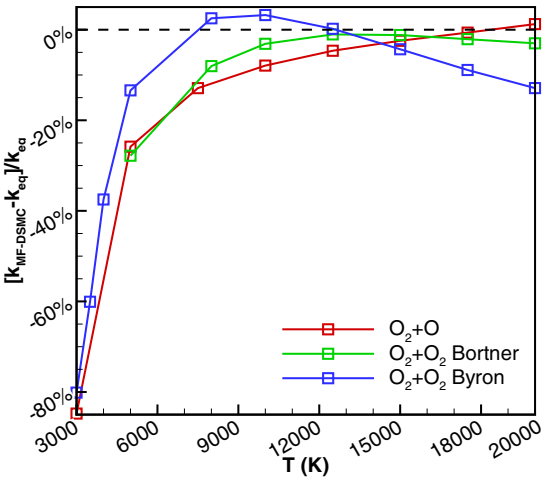

FIG. 20. Relative error of equilibrium dissociation rates calculated with the MF-DSMC and cVHS model to the baseline data.

dissociation rates combined with the MF-DSMC model. Kulakhmetov *et al.*'s QCT calculated rates for $O_2 + O$ [19], Byron's experimentally measured rates for $O_2 + O_2$ [51], and Bortner's estimations for $O_2 + O_2$ [56] are used as the baseline data to optimize the parameters. As shown in Fig. 20, the relative error of rate constants is within 15% for $T > 5000$ K. However, the DSMC implementation underestimates the rates at lower temperatures. Other symbols shown in Fig. 19 include R_i, representing different random numbers uniformly distributed between 0 and 1, and P_i, which are the probabilities for different procedures including collision, vibrational-translational (VT) relaxation, rotational-translational (RT) relaxation, and scattering. The definitions of these probabilities are shown as labels below the corresponding procedure. Z_v and Z_R are the VT and RT relaxation number, respectively, which are first calculated as the ratio of relaxation time and mean collision time of cVHS model, then corrected with Gimelshein *et al.*'s method [66] to fix the inconsistency between CFD and DSMC definitions of the relaxation collision numbers. The stagnation streamline approach [8] is used to stabilize the traveling shock. Details of the method can be found in previous work [64].

We select three different combinations of modeling parameters to simulate the O_2-reacting shock. A standard LB model is employed to describe VT relaxation for O_2-O_2 and RT relaxation for both O_2-O_2 and O_2-O. Kulakhmetov *et al.*'s ME-QCT-VT state-specific model [19] is used for O_2-O VT energy exchange. Since the VT cross sections σ_{VT} can be directly calculated with the model, there is no need for a relaxation time or relaxation number. For O_2-O_2, two different sets of vibrational relaxation time τ_v are used, and they are listed in Table III. Ibraguimova *et al.*'s model [27] is a fit to their experimental measurements. Andrienko *et al.* [63] used the forced harmonic oscillator (FHO) model [67] with master equations to calculate the relaxation time. Therefore, their results account for both VT and vibrational-vibrational (VV) processes. The values of the above two sets of vibrational relaxation time are compared with experimental measurements [27,68] and DMS

TABLE III. Different simulation frameworks.

	Model 1	Model 2	Model 3
τ_v: $O_2 - O_2$	Ibraguimova *et al.* [27]	Ibraguimova *et al.* [27]	Andrienko *et al.* [63]
$k_{eq}(T)$: $O_2 - O_2$	Byron [51]	Bortner [56]	Bortner [56]

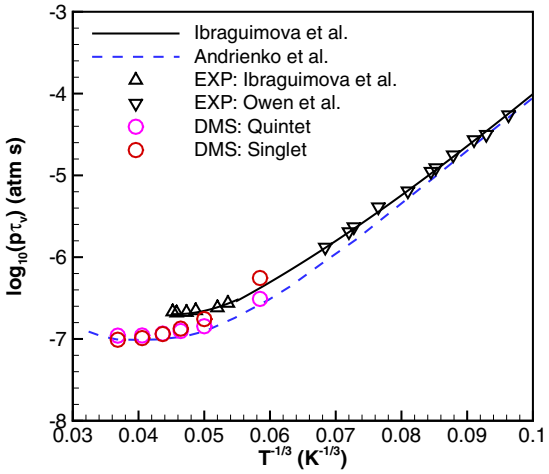

FIG. 21. Comparison of the VT relaxation time for O_2-O_2.

calculations [38] in Fig. 21. The values are close to each other at low temperatures, but Andrienko *et al.*'s model matches DMS calculations better at higher temperatures. MF-DSMC model is the only reaction model for the simulations. All the models reproduce Kulakhmetov *et al.*'s rate constants for O_2 dissociation in collisions with atomic oxygen, but they have different equilibrium reaction rates for $O_2 + O_2$ as listed in Table III.

The comparison of flow properties including temperatures, density, and mass fraction of O_2 is shown in Figs. 22–24. In addition to Ibraguimova *et al.*'s experimental measurements [27], the results of two state-specific simulations are also shown in these figures. Andrienko *et al.* [63] conduced master equation calculations with QCT VT and reaction rates for $O_2 + O$ and FHO VT rates for $O_2 + O_2$. Sebastião *et al.*'s framework of DSMC simulation (Model 4 in Ref. [64]) is very similar to Model 1 in this work except that they used the QCT state-specific $O_2 + O$ dissociation model [19] and calibrated the TCE model for the chemical reactions. These two calculations are believed to be the most state-of-art state-specific simulations and are compared to evaluate the MF-DSMC model.

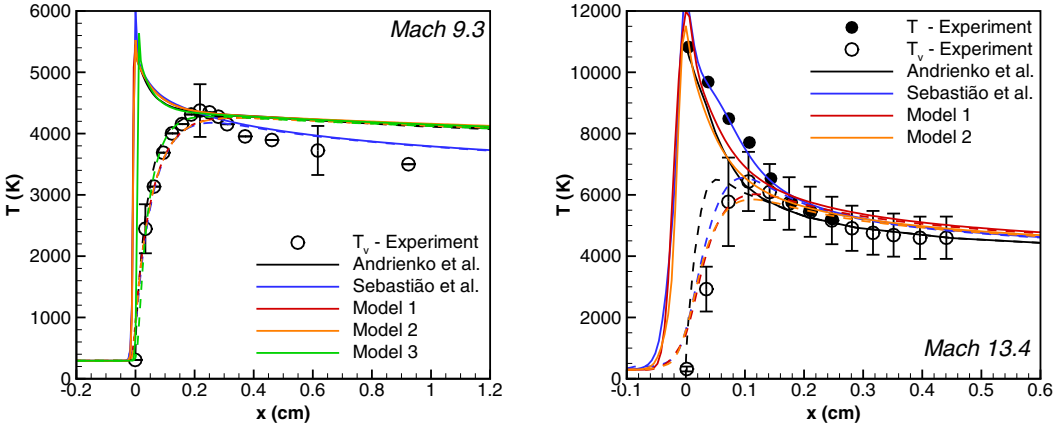

FIG. 22. Comparison of the temperature profile for the two cases. Solid lines for translational temperature; dashed lines for vibrational temperature.

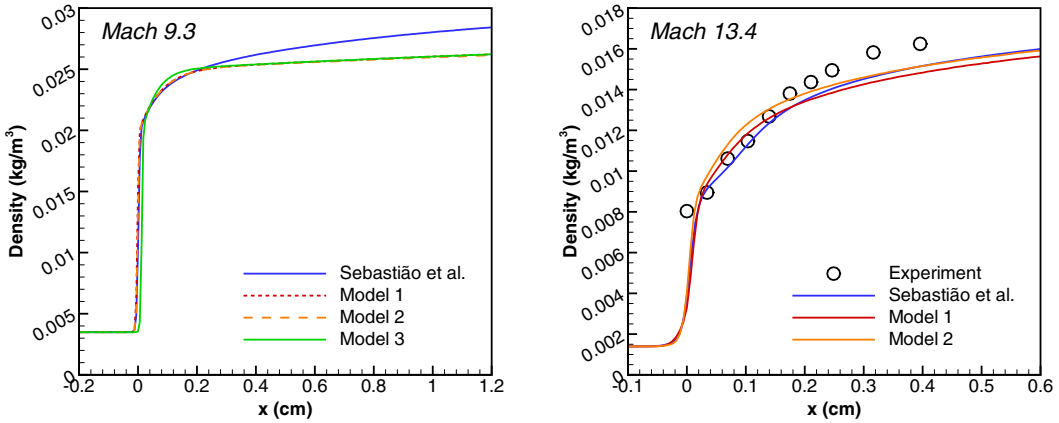

FIG. 23. Comparison of the density profile for the two cases.

For the Mach 9.3 case, Andrienko *et al.*'s calculations and Model 3 provide almost identical results. They reproduce the vibrational temperature profile before the peak T_v and the correct value of peak T_v. Models 1 and 2 along with Sebastião *et al.*'s simulations underpredict the values, but they are within the error bar of measurements. For the region after the peak T_v, only Sebastião *et al.*'s prediction of T_v is within the uncertainties. All other models underestimate the relaxation of temperatures. This can be understood with the help of comparisons of density and O_2 mass fraction in Figs. 23 and 24. It is seen that O_2 dissociation in Sebastião *et al.*'s calculations is more than twice as fast as that in the MF-DSMC simulations. The faster dissociation results in higher consumption of energy to break the O-O bond and therefore to faster drop of temperatures. Considering the underestimation of equilibrium dissociation rates for $T < 5000$ K shown in Fig. 20, we expect the simulation frameworks with MF-DSMC to reproduce the measurements better if the parameters of the cVHS model are further optimized. As an additional comment, the negligible difference between Models 1 and 2 is explained by the convergence of Bortner's and Byron's rate constants at low temperature (i.e., $T < 5000$ K).

For the Mach 13.4 case, Sebastião *et al.*'s simulations give the best agreement in terms of temperature and O_2 mass fraction. However, the models in this work also reproduce important features of the flow including thermal relaxation right after the shock front and downstream, the

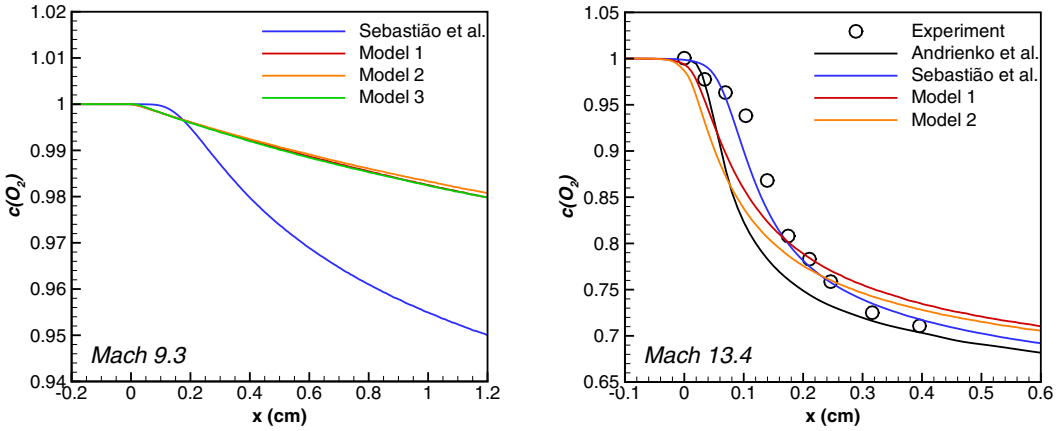

FIG. 24. Comparison of the O_2 mass fraction for the two cases.

profile of density, and the mass fraction of O_2 in the downstream. The models underpredict the peak T_v because the nonequilibrium factor for $O_2 + O_2$ is slightly higher than Sebastião *et al.*'s modeling. In addition, the average vibrational energy removed for O_2 dissociated by O_2 ranges between 1.5 and 3 eV for their simulations, which are below the values predicted by the MF-DSMC model as shown in Fig. 11.

In summary, it is not clear which model is the best one for the simulation due to the different performance for the two cases and the uncertainties of experimental measurements. What is clear is that MF-DSMC model can replace the QCT-based state-specific model for simulations of thermal-chemical nonequilibrium reactions without losing much accuracy. From the comparisons, we also see that VT relaxation plays a more important role at relatively low temperature where the rates of relaxation are higher than chemical reaction rates. In contrast, the chemical reaction dominates the energy relaxation behind the shock front at high temperatures.

VI. CONCLUSIONS

In this work, to develop a physics-based model of nonequilibrium dissociation for DSMC, we started from the MF theoretical model [20] based on the assumption of instantaneous classical collisions and proposed an implementation of the MF model in DSMC, the MF-DSMC model. The model was validated by comparison to recent QCT calculations. Very good agreement was obtained for vibrational state-specific reaction rates, nonequilibrium factors, and average vibrational energy removed by dissociation. Unlike the phenomenological TCE model, which is based on the inverse Laplace transform of Arrhenius reaction rates, the MF-DSMC model does not have adjustable parameters to match reaction rates. However, we found that although the MF model describing the dissociation probability once the collision occurs works well, the popular VHS model used in DSMC to calculate collision rates needs improvement. Indeed, due to the lower collision rates given by the VHS model, the absolute dissociation rate constants in MF-DSMC are lower than QCT data by up to an order of magnitude. To solve this problem, the parameters for calculating total cross section can be calibrated. A QCT-calibrated collision model was developed for a particular case of $N_2 + O$ collisions in this work. A more physical solution would require calculations of total collision cross sections from either QCT on *ab initio* PES or simplified collision dynamics based on model algebraic potential energy functions such as Lennard-Jones or Born-Mayer potentials.

The almost negligible difference in both equilibrium and nonequilibrium rates computed by MF-DSMC and QCT at high temperatures further confirms that collision-induced dissociation is not sensitive to the details of PES at conditions typical for hypersonic shock layers.

Finally, the MF-DSMC model was implemented in DS1V with a carefully tuned collision model and used to simulate the O_2 shockwave experiment [27]. Good agreement with the measurements as well as with previous state-specific numerical simulations [63,64] was obtained.

The present calculations and results indicate the potential of the model to be used as the standard DSMC dissociation reaction model.

[1] C. Park, *Nonequilibrium Hypersonic Aerothermodynamics* (Wiley, New York, 1990), pp. 171–218.
[2] H. H. Reising, K. C. Utsav, S. Voelkel, N. T. Clemens, V. Raman, P. L. Varghese, and H. Koo, Vibrational non-equilibrium effects in supersonic jet mixing, in *52nd AIAA Aerospace Sciences Meeting*, AIAA Paper 2014-0231 (2014).
[3] A. A. Fridman and L. A. Kennedy, *Plasma Physics and Engineering* (CRC Press, Boca Raton, FL, 2011).
[4] D. Yap, J.-M. Tatibouët, and C. Batiot-Dupeyrat, Carbon dioxide dissociation to carbon monoxide by non-thermal plasma, J. CO_2 Util. **12**, 54 (2015).
[5] C. Park, Review of chemical-kinetic problems of future NASA missions. I. Earth entries, J. Thermophys. Heat Transfer **7**, 385 (1993).

[6] P. V. Marrone and C. E. Treanor, Chemical relaxation with preferential dissociation from excited vibrational levels, Phys. Fluids **6**, 1215 (1963).
[7] O. Knab, H.-H. Fruehauf, and E. W. Messerschmid, Theory and validation of the physically consistent coupled vibration-chemistry-vibration model, J. Thermophys. Heat Transfer **9**, 219 (1995).
[8] G. A. Bird, *Molecular Gas Dynamics and the Direct Simulation of Gas Flows* (Oxford University Press, New York, 1994).
[9] I. D. Boyd, Analysis of vibration-dissociation-recombination processes behind strong shock waves of nitrogen, Phys. Fluids **4**, 178 (1992).
[10] I. J. Wysong and S. F. Gimelshein, Comparison of DSMC reaction models with QCT reaction rates for nitrogen, AIP Conf. Proc. **1786**, 050021 (2016).
[11] S. Gimelshein and I. Wysong, DSMC modeling of flows with recombination reactions, Phys. Fluids **29**, 067106 (2017).
[12] G. A. Bird, The Q-K model for gas-phase chemical reaction rates, Phys. Fluids **23**, 106101 (2011).
[13] M. Karplus, R. N. Porter, and R. D. Sharma, Exchange reactions with activation energy. I. Simple barrier potential for (H, H_2), J. Chem. Phys. **43**, 3259 (1965).
[14] D. G. Truhlar and J. T. Muckerman, Reactive scattering cross sections III: Quasiclassical and semiclassical methods, in *Atom-Molecule Collision Theory*, edited by R. B. Bernstein (Springer, Boston, MA, 1979), pp. 505–566.
[15] S. Kanne, O. Knab, H.-H. Fruehauf, M. Pogosbekyan, and S. A. Losev, Calibration of the CVCV-model against quasiclassical trajectory calculations, in *32nd Thermophysics Conference*, AIAA Paper 1997-2557 (1997).
[16] I. D. Boyd, D. Bose, and G. V. Candler, Monte Carlo modeling of nitric oxide formation based on quasi-classical trajectory calculations, Phys. Fluids **9**, 1162 (1997).
[17] O. Kunova, E. Kustova, and A. Savelev, Generalized Treanor-Marrone model for state-specific dissociation rate coefficients, Chem. Phys. Lett. **659**, 80 (2016).
[18] M. Panesi, R. L. Jaffe, D. W. Schwenke, and T. E. Magin, Rovibrational internal energy transfer and dissociation of $N_2(^1\Sigma_g^+)$-$N(^4S_u)$ system in hypersonic flows, J. Chem. Phys. **138**, 044312 (2013).
[19] M. Kulakhmetov, M. Gallis, and A. Alexeenko, *Ab initio*-informed maximum entropy modeling of rovibrational relaxation and state-specific dissociation with application to the O_2+O system, J. Chem. Phys. **144**, 174302 (2016).
[20] S. O. Macheret, A. A. Fridman, I. V. Adamovich, J. W. Rich, and C. E. Treanor, Mechanisms of nonequilibrium dissociation of diatomic molecules, in *6th Joint Thermophysics and Heat Transfer Conference*, AIAA Paper 1994-1984 (1994).
[21] S. O. Macheret and J. W. Rich, Nonequilibrium dissociation rates behind strong shock waves: Classical model, Chem. Phys. **174**, 25 (1993).
[22] S. O. Macheret and J. W. Rich, Theory of nonequilibrium dissociation rates behind strong shock waves, in *28th Thermophysics Conference*, AIAA Paper 1993-2860 (1993).
[23] G. G. Chernyi, S. A. Losev, S. O. Macheret, and B. V. Potapkin, *Physical and Chemical Processes in Gas Dynamics, Vol. I: Cross Sections and Rate Constants* (AIAA, Reston, Virginia, 2002), pp. 217–219.
[24] H. Luo, A. A. Alexeenko, and S. O. Macheret, Assessment of classical impulsive models of dissociation in thermochemical nonequilibrium, J. Thermophys. Heat Transfer **32**, 861 (2018).
[25] I. D. Boyd, A threshold line dissociation model for the direct simulation Monte Carlo method, Phys. Fluids **8**, 1293 (1996).
[26] D. C. Wadsworth and I. J. Wysong, Vibrational favoring effect in DSMC dissociation models, Phys. Fluids **9**, 3873 (1997).
[27] L. B. Ibraguimova, A. L. Sergievskaya, V. Y. Levashov, O. P. Shatalov, Y. V. Tunik, and I. E. Zabelinskii, Investigation of oxygen dissociation and vibrational relaxation at temperatures 4000–10,800 K, J. Chem. Phys. **139**, 034317 (2013).
[28] E. E. Nikitin, *Theory of Elementary Atomic and Molecular Processes in Gases* (Oxford University Press, Oxford, England, UK, 1974), p. 41.
[29] W. H. Miller, *Dynamics of Molecular Collisions*, edited by W. H. Miller (Springer, Boston, MA, 1976), pp. 32–36.

[30] M. Capitelli, C. Gorse, S. Longo, and D. Giordano, Collision integrals of high-temperature air species, J. Thermophys. Heat Transfer **14**, 259 (2000).
[31] F. Esposito, I. Armenise, G. Capitta, and M. Capitelli, O-O_2 state-to-state vibrational relaxation and dissociation rates based on quasiclassical calculations, Chem. Phys. **351**, 91 (2008).
[32] H. Luo, M. Kulakhmetov, and A. Alexeenko, *Ab initio* state-specific N_2+O dissociation and exchange modeling for molecular simulations, J. Chem. Phys. **146**, 074303 (2017).
[33] G. A. Bird, *The DSMC Method* (CreateSpace Independent Publishing Platform, North Charleston, SC, 2013).
[34] I. Wysong, S. Gimelshein, Y. Bondar, and M. Ivanov, Comparison of direct simulation Monte Carlo chemistry and vibrational models applied to oxygen shock measurements, Phys. Fluids **26**, 043101 (2014).
[35] R. Jaffe, D. Schwenke, and G. Chaban, Theoretical analysis of N_2 collisional dissociation and rotation-vibration energy transfer, in *47th AIAA Aerospace Sciences Meeting*, AIAA Paper 2009-1569 (2009).
[36] D. A. Andrienko and I. D. Boyd, State-resolved characterization of nitric oxide formation in shock flows, in *2018 AIAA Aerospace Sciences Meeting*, AIAA Paper 2018-1233 (2018).
[37] D. A. Andrienko and I. D. Boyd, Dissociation of oxygen and nitrogen in a bimolecular reaction at hypersonic temperatures, in *2018 AIAA Aerospace Sciences Meeting*, AIAA Paper 2018-0240 (2018).
[38] M. S. Grover and T. E. Schwartzentruber, Internal energy relaxation and dissociation in molecular oxygen using direct molecular simulation, in *47th AIAA Thermophysics Conference*, AIAA Paper 2017-3488 (2017).
[39] S. A. Losev, V. N. Makarov, M. J. Pogosbekyan, O. P. Shatalov, and V. S. Nikolsky, Thermochemical nonequilibrium kinetic models in strong shock waves on air, in *6th Joint Thermophysics and Heat Transfer Conference*, AIAA Paper 1994-1990 (1994).
[40] M. S. Yalovik and S. A Losev, Vibrational kinetics and dissociation of nitrogen molecules at high temperature, Scientific Proceedings, Institute of Mechanics, Moscow State University **18**, 3 (1972).
[41] J. D. Bender, P. Valentini, I. Nompelis, Y. Paukku, Z. Varga, D. G. Truhlar, T. Schwartzentruber, and G. V. Candler, An improved potential energy surface and multi-temperature quasiclassical trajectory calculations of $N_2 + N_2$ dissociation reactions, J. Chem. Phys. **143**, 054304 (2015).
[42] R. S. Chaudhry, J. D. Bender, T. E. Schwartzentruber, and G. V. Candler, Quasiclassical trajectory analysis of $N_2 + N_2$ and implications for hypersonic CFD, in *47th AIAA Thermophysics Conference*, AIAA Paper 2017-3167 (2017).
[43] R. S. Chaudhry, M. S. Grover, J. D. Bender, T. E. Schwartzentruber, and G. V. Candler, Quasiclassical trajectory analysis of oxygen dissociation via O_2, O, and N_2, in *2018 AIAA Aerospace Sciences Meeting*, AIAA Paper 2018-0237 (2018).
[44] F. Esposito, I. Armenise, and M. Capitelli, N-N_2 state to state vibrational-relaxation and dissociation rates based on quasiclassical calculations, Chem. Phys. **331**, 1 (2006).
[45] D. A. Andrienko and I. D. Boyd, Rovibrational energy transfer and dissociation in O_2-O collisions, J. Chem. Phys. **144**, 104301 (2016).
[46] F. Esposito and I. Armenise, Reactive, inelastic, and dissociation processes in collisions of atomic oxygen with molecular nitrogen, J. Phys. Chem. **121**, 6211 (2017).
[47] D. A. Andrienko and I. D. Boyd, State-specific dissociation in O_2-O_2 collisions by quasiclassical trajectory method, Chem. Phys. **491**, 74 (2017).
[48] S. Byron, Shock-tube measurement of the rate of dissociation of nitrogen, J. Chem. Phys. **44**, 1378 (1966).
[49] O. P. Shatalov, Molecular dissociation of oxygen in the absence of vibrational equilibrium, Combust. Explo. Shock Waves **9**, 610 (1973).
[50] J. P. Appleton, M. Steinberg, and D. J. Liquornik, Shock-tube study of nitrogen dissociation using vacuum-ultraviolet light absorption, J. Chem. Phys. **48**, 599 (1968).
[51] S. R. Byron, Measurement of the rate of dissociation of oxygen, J. Chem. Phys. **30**, 1380 (1959).
[52] L. Jerig, J. Thielen, and P. Roth, High-temperature dissociation of oxygen diluted in argon or nitrogen, AIAA J. **29**, 1136 (1991).
[53] N. A. Generalov and S. A. Losev, Vibration, excitation, and molecular dissociation of gaseous oxygen and carbon dioxide in a shock wave, J. Quant. Spectrosc. Radiat. Transfer **6**, 101 (1966).

[54] O. P. Shatalov, Recommended data on rate constants of physical and chemical processes in N–O atoms system, Tech. Rep. (1987).
[55] D. L. Baulch, D. D. Drysdale, J. Duxbury, and S. J. Grant, *Evaluated Kinetic Data for High Temperature Reactions, Vol. 3: Homogeneous Gas Phase Reactions of the O_2-O_3 System* (Butterworths, London, 1976), p. 595.
[56] M. H. Bortner, A review of rate constants of selected reactions of interest in re-entry flow fields in the atmosphere, Tech. Rep., National Bureau of Standards (1969).
[57] K. L. Wray, Chemical kinetics of high temperature air, in *Hypersonic Flow Research*, edited by F. R. Riddell (Academic Press, London, UK, 1962), pp. 181–204.
[58] A. B. Weaver and A. A. Alexeenko, Revised variable soft sphere and Lennard-Jones model parameters for eight common gases up to 2200 K, J. Phys. Chem. Ref. Data **44**, 023103 (2015).
[59] K. Koura and H. Matsumoto, Variable soft sphere molecular model for inverse-power-law or Lennard-Jones potential, Phys. Fluids **3**, 2459 (1991).
[60] T. Zhu, Z. Li, and D. A. Levin, Development of a two-dimensional binning model for N_2-N relaxation in hypersonic shock conditions, J. Chem. Phys. **145**, 064302 (2016).
[61] J. Kim and I. D. Boyd, State resolved thermochemical modeling of nitrogen using DSMC, in *43rd AIAA Thermophysics Conference*, AIAA Paper 2012-2991 (2012).
[62] W. L. Dimpfl, I. J. Wysong, S. F. Gimelshein, M. Braunstein, and L. S. Bernstein, Application of the Born-Mayer potential with a hard-sphere scattering kernel to rarefied hyperthermal gas flow modeling, AIP Conf. Proc. **1084**, 323 (2008).
[63] D. A. Andrienko and I. D. Boyd, Vibrational relaxation and dissociation in O_2-O mixtures, in *46th AIAA Thermophysics Conference*, AIAA Paper 2016-4021 (2016).
[64] I. B. Sebastião, M. Kulakhmetov, and A. Alexeenko, DSMC study of oxygen shockwaves based on high-fidelity vibrational relaxation and dissociation models, Phys. Fluids **29**, 017102 (2017).
[65] E. Kustova, E. Nagnibeda, G. Oblapenko, A. Savelev, and I. Sharafutdinov, Advanced models for vibrational–chemical coupling in multi-temperature flows, Chem. Phys. **464**, 1 (2016).
[66] N. E. Gimelshein, S. F. Gimelshein, and D. A. Levin, Vibrational relaxation rates in the direct simulation Monte Carlo method, Phys. Fluids **14**, 4452 (2002).
[67] I. V. Adamovich, S. O. Macheret, J. W. Rich, and C. E. Treanor, Vibrational energy transfer rates using a forced harmonic oscillator model, J. Thermophys. Heat Transfer **12**, 57 (1998).
[68] K. G. Owen, D. F. Davidson, and R. K. Hanson, Oxygen vibrational relaxation times: Shock tube/laser absorption measurements, J. Thermophys. Heat Transfer **30**, 791 (2016).